View metadata, citation and similar papers at core.ac.uk

brought to you by CORE

provided by Apollo

PHYSICAL REVIEW B **101**, 241405(R) (2020)

Rapid Communications | Editors' Suggestion

Transition between canted antiferromagnetic and spin-polarized ferromagnetic quantum Hall states in graphene on a ferrimagnetic insulator

Yang Li,[1,2,*] Mario Amado,[1,*] Timo Hyart,[3] Grzegorz P. Mazur,[3] Vetle Risinggård,[4,5] Thomas Wagner,[1,6] Lauren McKenzie-Sell,[1,7] Graham Kimbell,[1] Joerg Wunderlich,[6,8,9] Jacob Linder,[4,5] and Jason W. A. Robinson[1,†]

[1]*Department of Materials Science & Metallurgy, University of Cambridge, 27 Charles Babbage Road, Cambridge CB3 0FS, United Kingdom*

[2]*Cambridge Graphene Centre, University of Cambridge, 9 JJ Thomson Avenue, Cambridge CB3 0FA, United Kingdom*

[3]*International Research Centre MagTop, Institute of Physics, Polish Academy of Sciences, Aleja Lotników 32/46, PL-02668 Warsaw, Poland*

[4]*Department of Physics, Norwegian University of Science and Technology, NO-7491 Trondheim, Norway*

[5]*Center for Quantum Spintronics, Department of Physics, Norwegian University of Science and Technology, NO-7491 Trondheim, Norway*

[6]*Hitachi Cambridge Laboratory, Cambridge CB3 0HE, United Kingdom*

[7]*Cavendish Laboratory, University of Cambridge, Cambridge CB3 0HE, United Kingdom*

[8]*Institute of Experimental and Applied Physics, University of Regensburg, Universitätsstrasse 31, 93051 Regensburg, Germany*

[9]*Institute of Physics, Czech Academy of Sciences, Cukrovarnicka 10, 162 00, Praha 6, Czech Republic*

(Received 14 June 2019; revised manuscript received 8 October 2019; accepted 22 April 2020; published 1 June 2020)

In the quantum Hall regime of graphene, antiferromagnetic and spin-polarized ferromagnetic states at the zeroth Landau level compete, leading to a canted antiferromagnetic state depending on the direction and magnitude of an applied magnetic field. Here, we investigate this transition at 2.7 K in graphene Hall bars that are proximity coupled to the ferrimagnetic insulator $Y_3Fe_5O_{12}$. From nonlocal transport measurements, we demonstrate an induced magnetic exchange field in graphene, which lowers the magnetic field required to modulate the magnetic state in graphene. These results show that a magnetic proximity effect in graphene is an important ingredient for the development of two-dimensional materials in which it is desirable for ordered states of matter to be tunable with relatively small applied magnetic fields (>6 T).

DOI: 10.1103/PhysRevB.101.241405

Graphene has two inequivalent Dirac cones in the energy band dispersion, which lead to a set of Landau levels with distinct features over conventional two-dimensional electron gases, e.g., in an applied magnetic field ($\boldsymbol{B}$), there exists fourfold degenerate symmetry-broken zero-energy Landau levels with filling factors $\upsilon = 0$ and ± 1 [1–3]. These are gate-voltage tunable and described by spin and valley degeneracy. Electron-electron and electron-phonon interactions break valley symmetry and determine the magnetic order of the $\upsilon = 0$ state. Theory [4–6] and experiment [7–10] indicate that $\upsilon = 0$ is an antiferromagnetic (AF) quantum Hall state [6,9] in which the two sublattice spins of graphene align antiparallel. The Zeeman field associated with an in-plane magnetic field ($B_\parallel$) favors a spin-polarized ferromagnetic (F) state [9] (that can be also found at $\upsilon = \pm 1$ [7]), but in general the AF and F states compete, leading to a canted antiferromagnetic (CAF) $\upsilon = 0$ state at a half-filled zero-energy Landau level in which the two sublattice spins tilt out of plane. The spin direction in the CAF state depends on the sum of the spin components parallel (preferred by the Zeeman field, responsible for the F state) and perpendicular to $\boldsymbol{B}$ (preferred by the electron-electron Coulomb interactions responsible for the valley anisotropy and leading to the AF state). In the AF state, there are gapped edge modes while the F state supports gapless counterpropagating edge modes [5,7,11]. Therefore, in the CAF state the energy gap of the edge modes is tunable with the direction and magnitude of $\boldsymbol{B}$ [5].

Edge modes associated with CAF and F states have been detected in graphene Hall bars through nonlocal measurements with a transition between F and CAF states occurring around 15–30 T [9]. In the ballistic limit, the nonlocal resistance ($R_{\rm nl}$) is quantized and dependent on the Hall bar geometry [12]. In the diffusive limit, $R_{\rm nl}$ is not quantized but shows different behaviors with gate voltage ($V_{\rm TG}$) in the AF, CAF, and F states [Figs. 1(a)–1(c)]: The AF state does not support edge modes, meaning $R_{\rm nl} = 0$, but the CAF (F) is gapped (gapless) and $R_{\rm nl}$ shows a double peak (single peak) around the Dirac point ($V_{\rm D}$).

Transitions between CAF and F (or AF) states could be achieved in lower applied magnetic fields if graphene has an intrinsic magnetic exchange field ($\boldsymbol{M}_{\rm ex}$). By placing graphene on an insulating magnetic substrate, a hybridization of the π orbitals in graphene with the substrate can theoretically induce a magnetic exchange field of hundreds of tesla [13–18]. The magnitude of the total magnetic field ($M_{\rm T} = \|\boldsymbol{M}_{\rm T}\|$) applied to graphene is then related to $\boldsymbol{M}_{\rm T} = \frac{g}{2}\boldsymbol{B} + \boldsymbol{M}_{\rm ex}$, where g is gyromagnetic ratio and $\frac{g}{2}\boldsymbol{B}$ is the Zeeman field. $\boldsymbol{M}_{\rm ex}$ is parallel to $\boldsymbol{B}$. A 14-T magnetic exchange field was recently estimated in graphene on EuS [14] and an anomalous Hall effect in graphene on $Y_3Fe_5O_{12}$ (YIG) showed evidence for

*These authors contributed equally to this work.

†Corresponding author: jjr33@cam.ac.uk

 ©2020 American Physical Society

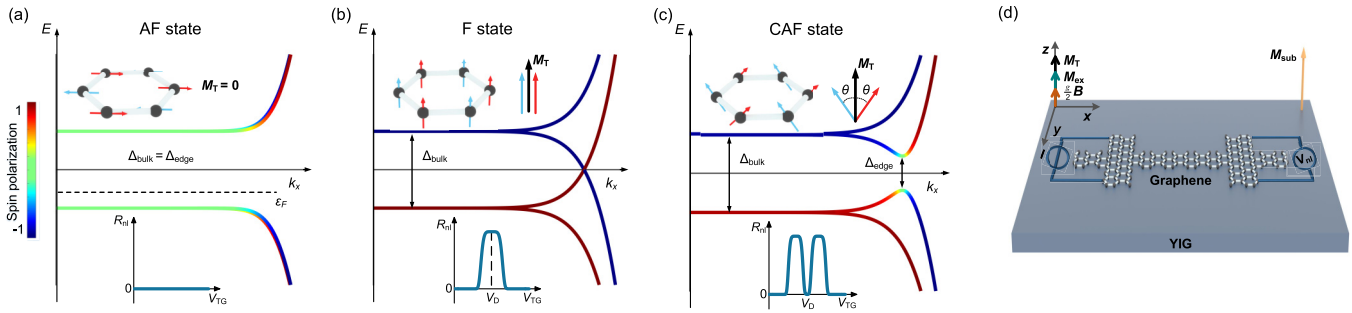

FIG. 1. Energy spectra for the (a) AF, (b) F, and (c) CAF states in graphene, which arise depending on the total magnetic field ($\boldsymbol{M}_\mathbf{T}$) applied to graphene and the angle (θ) between $\boldsymbol{M}_\mathbf{T}$ and the sublattice spins. Color scale bar shows -1 (spin direction antiparallel to $\boldsymbol{M}_\mathbf{T}$) to 1 (spin direction parallel to $\boldsymbol{M}_\mathbf{T}$). Top insets in (a)–(c): Schematic diagrams illustrating the sublattice spins in graphene (left) which make an angle θ with respect to $\boldsymbol{M}_\mathbf{T}$ (right). Bottom insets in (a)–(c): $R_{\rm nl}$ vs $V_{\rm TG}$ for AF, F, and CAF states near $V_{\rm D}$. (a) The AF state forms when $\boldsymbol{M}_\mathbf{T}$ is zero (sublattice spins are antiparallel). (b) The F state forms when $\boldsymbol{M}_\mathbf{T}$ is larger than a critical value (determined by the Coulomb interaction) and the sublattice spins are parallel to $\boldsymbol{M}_\mathbf{T}$. (c) The CAF state is a mixture of AF and F states and forms when $\boldsymbol{M}_\mathbf{T}$ is nonzero, but smaller than a critical value (sublattice spins are noncollinear to $\boldsymbol{M}_\mathbf{T}$). (d) Schematic diagram of a graphene Hall bar on YIG in which the YIG magnetization ($\boldsymbol{M}_\mathbf{sub}$) induces a nonzero $\boldsymbol{M}_\mathbf{ex}$ in graphene that adds to the Zeeman field ($\frac{g}{2}\boldsymbol{B}$).

an induced magnetic exchange field in graphene [19]. In Refs. [14,19], transitions between CAF and F (or AF) states were not investigated.

Here, we report transitions between CAF and F states in hexagonal boron nitride (hBN) covered graphene Hall bars on YIG. These are investigated through gate-voltage-dependent nonlocal transport measurements below 9 K. The magnetic state and energy gap of the edge modes in graphene are tunable by varying the magnitude (>6 T) and direction of an applied magnetic field ($\boldsymbol{B}$). The tunable energy gap is important from a fundamental viewpoint, as it separates quantum states with distinct magnetic ordering in graphene, and implies potential relevance for applications requiring a tunable band gap, such as photodetectors.

YIG has a Curie temperature of 550 K, a band gap of 2.84 eV, and an electrical resistivity of $10^{12}\,\Omega\,$cm. Moreover, it is chemically stable in air, which minimizes surface degradation during Hall bar fabrication. Atomically flat (1 1 0) YIG (84-nm-thick) is prepared by pulsed laser deposition onto gadolinium gallium garnet (GGG) [Fig. 2(a) and bottom inset] with a bulk magnetization of 144 emu cm^{-3} [see Fig. S3 in the Supplemental Material (SM) [21]]. Hall bars are fabricated in several steps, in which graphene is exfoliated from graphite and transferred onto YIG. The graphene is covered with a 20-to-50-nm-thick layer of hBN and electron beam lithography defines the Cr/Au side contacts [21]. In this Rapid Communication, we report two hBN/graphene Hall bars on YIG, which show a field-effect mobility (μ) of around 12 000 cm^2 V^{-1} s^{-1} (device I) and 10 000 cm^2 V^{-1} s^{-1} (device II) at 9 K. The control Hall bar of hBN/graphene/AlO$_x$/YIG ($\mu \approx 15\,000\,$cm^2 V^{-1} s^{-1} at 9 K) is investigated in which graphene is decoupled from YIG with a 6-nm-thick AlO$_x$ layer. Raman spectroscopy is performed on the graphene prior to and following transfer onto YIG or AlO$_x$ [top inset in Fig. 2(a)] and shows no evidence for defects in graphene.

Figure 2(b) (left inset) shows a representative hBN/graphene Hall bar on YIG prior to top-gate electrode deposition. Resistance is measured using lock-in amplifiers [21]. For local transport, $I_{9,10}$ indicates current flowing between contacts 9 and 10 and a local voltage $V_{3,5}$ is measured between contacts 3 and 5, giving $R_{xx} = V_{3,5}/I_{9,10}$. The nonlocal voltage

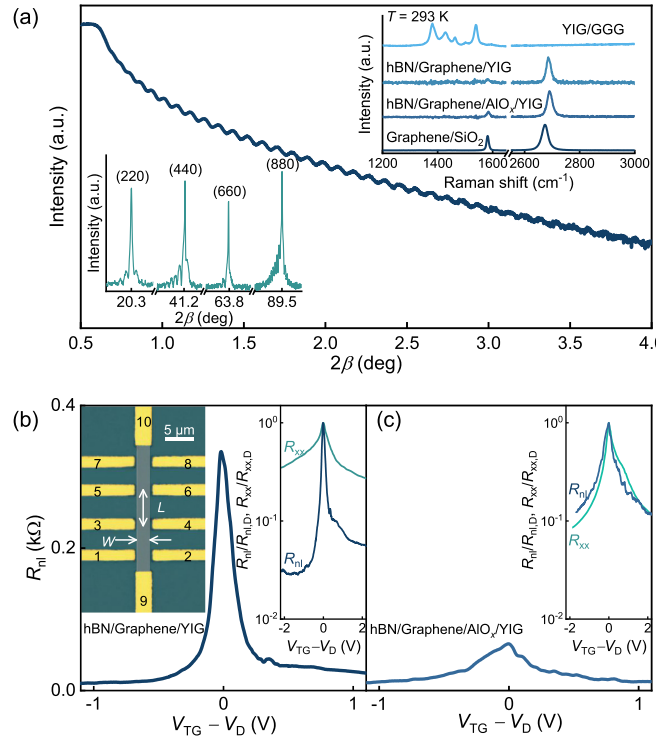

FIG. 2. (a) X-ray reflectivity of YIG (84-nm-thick with a roughness of 0.14 nm) on GGG. Upper inset: Raman spectra at 293 K for different structures (labeled) in which the background Raman spectra from hBN and YIG/GGG are subtracted. The G-peak (≈1580 cm^{-1}) and 2D-peak (≈2700 cm^{-1}) positions of graphene on different substrates vary due to different doping levels [20]. Lower inset: X-ray diffraction trace showing single-phase (1 1 0) YIG. (b), (c) $R_{\rm nl}$ vs $V_{\rm TG} - V_{\rm D}$ at 9 K for an hBN/graphene Hall bar on YIG (device I) and a control Hall bar (labeled) with insets (right) showing $R_{xx}/R_{xx,\rm D}$ and $R_{\rm nl}/R_{\rm nl,D}$ vs $V_{\rm TG} - V_{\rm D}$ for the same Hall bar in zero magnetic field. Left inset of (b): False color optical image of an hBN/graphene Hall bar on YIG.

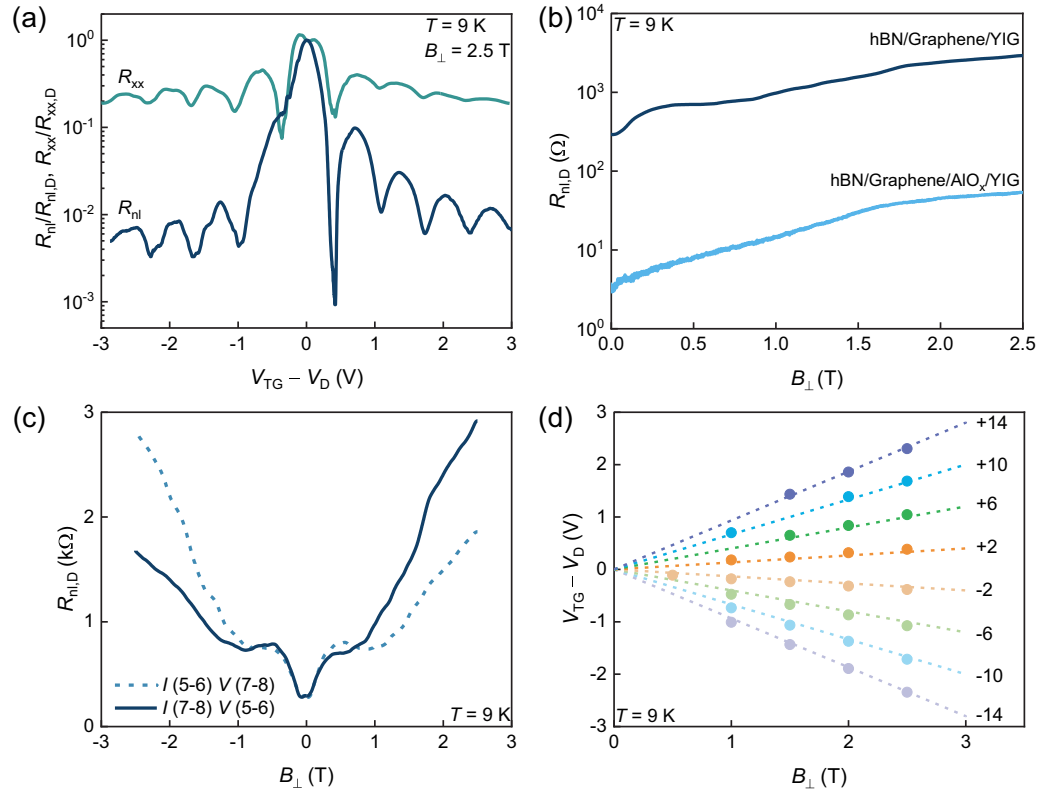

FIG. 3. (a) Gate-voltage dependence of $R_{xx}/R_{xx,\mathrm{D}}$ and $R_{\mathrm{nl}}/R_{\mathrm{nl,D}}$ with $B_\perp = 2.5\,\mathrm{T}$. (b) $R_{\mathrm{nl,D}}$ with $B_\perp$ for device I compared to the hBN/graphene/AlO_x/YIG control Hall bar. (c) $R_{\mathrm{nl,D}}$ vs $B_\perp$ for reverse electrical connections showing that the Onsager relation is obeyed in device I. (d) Landau level fan diagram where the dashed lines are calculated fitting results. Filling factors are shown beside the dashed lines. All data are recorded at 9 K.

is probed away from the current path (e.g., $R_{\mathrm{nl}} = R_{34,56} = V_{5,6}/I_{3,4}$).

We first discuss the transport properties in zero magnetic field for device I at 9 K. Figure 2(b) shows a peak in R_{nl} at V_{D}. By normalizing R_{xx} and R_{nl} to their maximum values at V_{D} ($R_{xx,\mathrm{D}}$ or $R_{\mathrm{nl,D}}$), we see that $R_{\mathrm{nl}}/R_{\mathrm{nl,D}}$ is an order of magnitude smaller than $R_{xx}/R_{xx,\mathrm{D}}$ and the peak in R_{nl} is sharper than R_{xx} [right inset in Fig. 2(b)]. The peak in R_{nl} ($\approx$380 Ω) at V_{D} may indicate a contribution from the spin Hall [22] or Zeeman spin Hall effects [14]. However, R_{xx} shows a negative magnetoresistance (weak localization) [see Fig. S5(b) in SM [21]] at 2.7 K, suggesting that Rashba spin-orbit coupling is not strong at the graphene/YIG interface, and meaning that the spin Hall effect is unlikely to dominate R_{nl}. The YIG has a small remanent out-of-plane magnetic moment [see Fig. S3(d) in SM [21]] which may support the Zeeman spin Hall effect. We note that ohmic, Joule heating, and Ettingshausen contributions to R_{nl} are negligible [21]. Equivalent measurements on an hBN/graphene/AlO_x/YIG control Hall bar [Fig. 2(c)] show a reduced R_{nl} at V_{D} of around 65 Ω at 9 K, which is dominated by the ohmic effect. This suggests that in zero magnetic field, $R_{\mathrm{nl,D}}$ of device I is due to a coupling between graphene and YIG.

In Fig. 3(a) we show gate-voltage-dependent Shubnikov–de Haas oscillations in R_{xx} and R_{nl} (normalized to values at V_{D}) for device I with an out-of-plane magnetic field of 2.5 T. The ratios $R_{\mathrm{nl}}/R_{\mathrm{nl,D}}$ and $R_{xx}/R_{xx,\mathrm{D}}$ show different trends with gate voltage with R_{nl} decreasing faster than R_{xx}. Furthermore, the value of R_{nl} is a factor of 50 larger than in the hBN/graphene/AlO_x/YIG control Hall bar [Fig. 3(b)]. These observations, in conjunction with the fact that the Onsager relation $R_{56,78}(B_\perp) = R_{78,56}(-B_\perp) \neq R_{78,56}(B_\perp)$ for device I holds [Fig. 3(c)], demonstrate a contribution to R_{nl} from the Zeeman spin Hall effect [14,23] due to an induced magnetic exchange field. Shubnikov–de Haas oscillations are observed for $B_\perp \geqslant 1\,\mathrm{T}$ (see Fig. S6 in SM [21]), showing Landau levels at filling factors $\nu = 4(N + 1/2)$ where $N = 0, \pm1, \pm2\ldots$ [Fig. 3(d)]. In addition, the induced magnetic exchange field manifests through the appearance of an anomalous Hall effect in Fig. S9 [21].

For large $B_\perp$, quantum Hall plateaus at $\nu = 0$ and ±1 may become visible. The $\nu = 0$ state at the half-filled zeroth Landau level should show a minimum in longitudinal conductance (σ_{xx}) while the other filling factors at a quarter and three-quarter occupancy are at a maximum. In Figs. 4(a)–4(d) we show the dependence of σ_{xx} on gate voltage for increasing values of $B_\perp$: In 4 T a minimum in σ_{xx} is visible at V_{D} and approaches zero in 12 T. Over the same magnetic field range at V_{D}, $\rho_{xx,\mathrm{D}}$ rapidly increases [inset of Fig. 4(d)], indicating a transition to a gapped bulk state. Simultaneously, the Hall conductance (σ_{xy}) tends to be a plateau establishing the $\nu = 0$ state. We note that equivalent measurements on the hBN/graphene/AlO_x/YIG control Hall bar do not show these trends [21], indicating that a coupling between graphene and YIG reduces $B_\perp$ to achieve the $\nu = 0$ state.

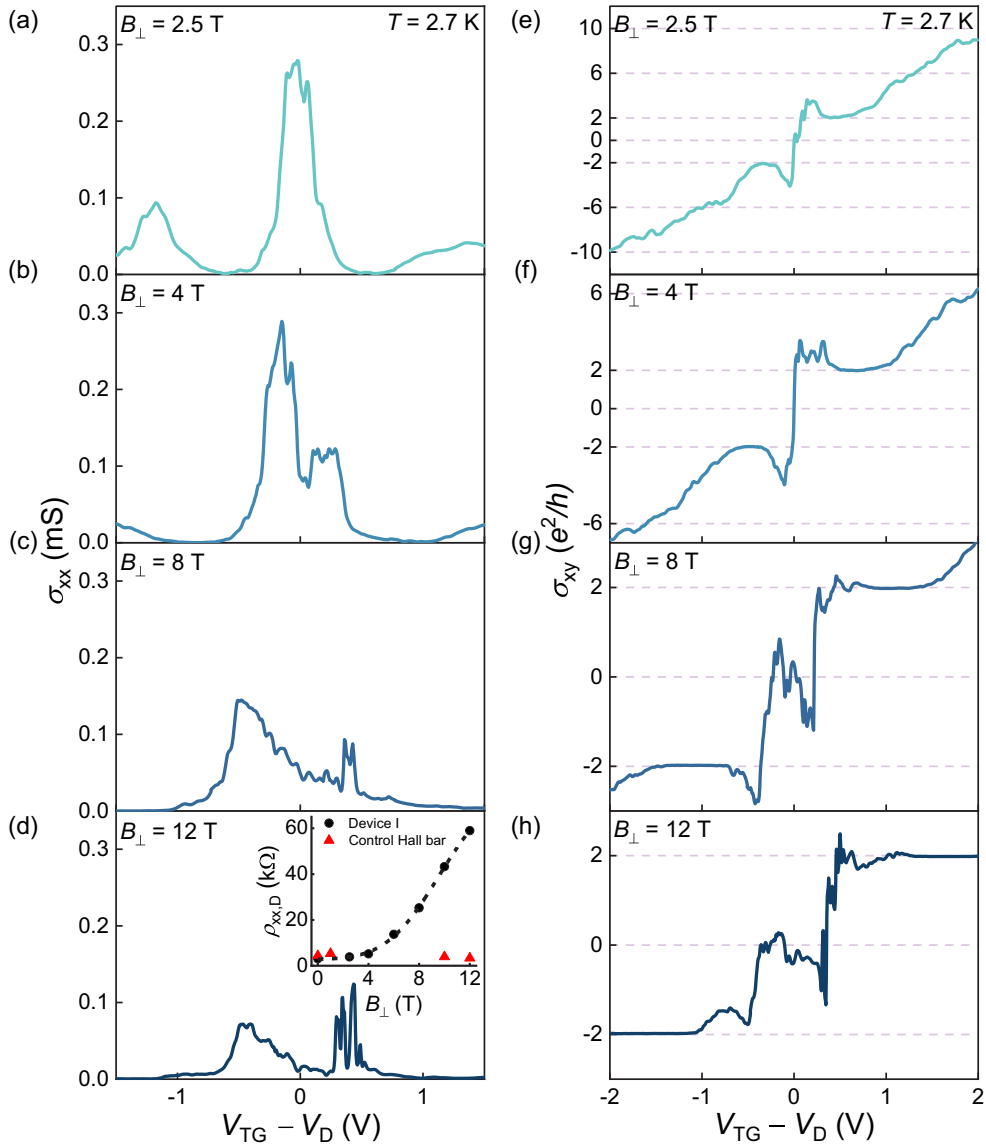

FIG. 4. (a)–(d) Gate-voltage dependence of the longitudinal conductance (σ_{xx}) for increasing $B_\perp$ (labeled) and (e)–(h) the corresponding Hall conductance (σ_{xy}) over the same magnetic field range. Inset of (d) shows the longitudinal resistivity ($\rho_{xx,D}$) at V_D vs $B_\perp$ for device I and the hBN/graphene/AlO_x/YIG control Hall bar. All data are recorded at 2.7 K.

The $\upsilon = 0$ state in Fig. 4 could be a F or a CAF state. These are distinguishable from the gate-voltage dependence of R_{nl} with $B_\perp$ as shown in Figs. 5(a)–5(c) for device I and Figs. 5(d)–5(f) for device II; the transition from a single to a double peak in R_{nl} with gate voltage suggests that the $\upsilon = 0$ state is associated with a transition from the F to CAF state. Although consistent with theory [5], the transition occurs in graphene at lower values of $B_\perp$ than without YIG (>15 T in Ref. [9]). Furthermore, the decrease in R_{nl} at V_D with increasing $B_\perp$ suggests an increase in the edge gap and the angle between $\boldsymbol{M}_T$ and the sublattice spins [21]. This angle increases with $B_\perp$ because the valley anisotropy energy (which resulted from electron-electron interactions, which leads to an AF state) increases faster than the Zeeman energy, as discussed in SM [21]. To test this hypothesis, we rotated device II from $\alpha = 90^\circ$ to $\alpha = 0^\circ$ using magnetic fields of 2–12 T, where α is the angle between the Hall bar surface and $\boldsymbol{B}$ [Fig. 5(g)]. This rotation partially (6 T < $\|\boldsymbol{B}\|$ < 12 T) or fully ($\|\boldsymbol{B}\|$ = 12 T) transforms the CAF to F state. As the fixed B rotates in plane, $B_\perp$ decreases and the sublattice spins align to $\boldsymbol{M}_T$, reducing the edge gap and increasing $R_{nl,D}$.

Transitions between CAF and F states were investigated in Ref. [9] using hBN/graphene Hall bars with rotating $\boldsymbol{B}$ up to 35 T at 300 mK. In that work the graphene was not in contact with a magnetic substrate, meaning $\|\boldsymbol{M}_{ex}\| = 0$ and thus there is only a Zeeman field. By extracting the average values of M_T vs $B_\perp$ in Ref. [9], we calculate a phase transition line of $M_T \approx 9.9B_\perp + 4.9$ which separates the CAF and F states as shown in Fig. 5(h) and explained in SM [21]. For devices I and II [Figs. 5(a)–5(f)], transitions between the CAF and F states

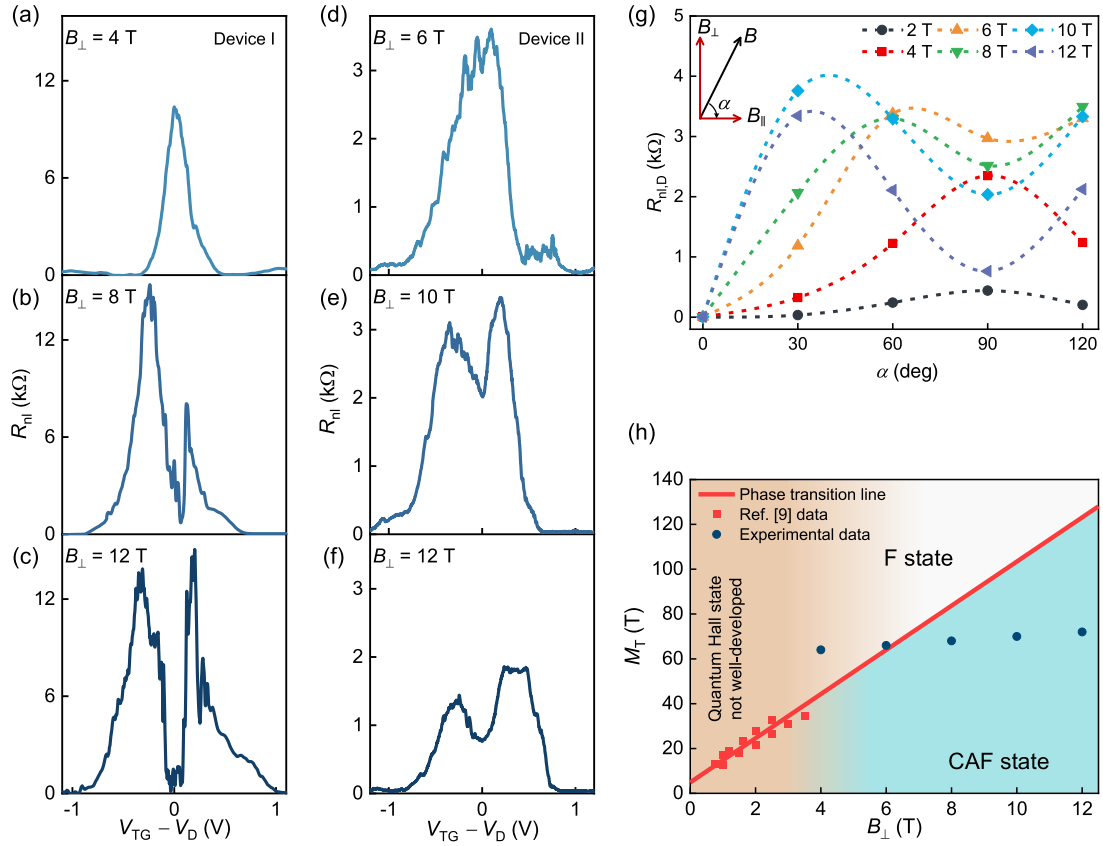

FIG. 5. (a)–(f) Gate-voltage dependence of R_{nl} for different values of $B_\perp$ (labeled) for (a)–(c) device I and (d)–(f) device II. (g) $R_{nl,D}$ vs α with $\boldsymbol{B}$ from 2 to 12 T for device II. Dashed lines are a guide to the eye. A $\pm 5°$ operational error due to manual rotation of the sample holder leads to the small asymmetry in $R_{nl,D}$ at $\alpha = 60°$ and 120°. (h) Magnetic phase diagram (M_T vs $B_\perp$) for graphene in which the solid (red) line $M_T \approx 9.9B_\perp + 4.9$ is calculated from Ref. [9] using the extracted data in red as explained in the main text and SM [21]. The blue data represent the estimated phases for devices I and II with $B_\perp$ only. For small $B_\perp$, the quantum Hall state is not well developed. By increasing $B_\perp$, there exists a transition between the F and CAF state. For reasonably small $B_\perp$ and large M_T, the F state is realized, whereas by increasing the ratio of $B_\perp/M_T$, the CAF state becomes energetically favored. All data are recorded at 2.7 K except the data from Ref. [9], which are at 300 mK.

occur from $B_\perp > 6$ T. By comparing our results with Ref. [9] and using $\boldsymbol{M_T} = \frac{g}{2}\boldsymbol{B} + \boldsymbol{M_{ex}}$, we estimate M_{ex} in graphene to be of the order 60 T due to the magnetic proximity effect. This estimate assumes that M_{ex} is independent of $\boldsymbol{B}$ as long as B is enough to fully magnetize YIG (which is the case in our experiment) [21].

In conclusion, we have demonstrated that by proximity inducing a magnetic exchange field in graphene on a ferrimagnetic substrate, transitions between CAF and F states can be achieved with relatively low applied magnetic fields (>6 T) at 2.7 K. This achievement is important for the development of two-dimensional materials with magnetic-field-tunable ordered states of matter.

The work was funded by the Royal Society and the Engineering and Physical Sciences Research Council (EPSRC, Grant No. EP/P026311/1). Y.L. was supported by the China Scholarship Council (CSC) Cambridge International Scholarship. J.L. and V.R. received funding from the Outstanding Academic Fellows Program at the NTNU, the NV-Faculty, and the Research Council of Norway (Grants No. 216700 and No. 240806) and funding for the Centre of Excellence QuSpin (Grant No. 262633). T.H. and G.P.M. were supported by the Foundation for Polish Science through the IRA Programme cofinanced by EU within SG OP. G.P.M. was supported by the National Science Center (Poland) through ETIUDA fellowship (Grant No. UMO-2017/24/T/ST3/00501).

[1] A. H. Castro Neto, F. Guinea, N. M. R. Peres, K. S. Novoselov, and A. K. Geim, Rev. Mod. Phys. **81**, 109 (2009).
[2] K. Nomura and A. H. MacDonald, Phys. Rev. Lett. **96**, 256602 (2006).
[3] K. Yang, S. Das Sarma, and A. H. MacDonald, Phys. Rev. B **74**, 075423 (2006).
[4] M. Kharitonov, Phys. Rev. B **85**, 155439 (2012).
[5] M. Kharitonov, Phys. Rev. B **86**, 075450 (2012).
[6] B. Feshami and H. A. Fertig, Phys. Rev. B **94**, 245435 (2016).
[7] D. S. Wei, T. van der Sar, S. H. Lee, K. Watanabe, T. Taniguchi, B. I. Halperin, and A. Yacoby, Science **362**, 229 (2018).
[8] A. F. Young, C. R. Dean, L. Wang, H. Ren, P. Cadden-Zimansky, K. Watanabe, T. Taniguchi, J. Hone, K. L. Shepard, and P. Kim, Nat. Phys. **8**, 550 (2012).

[9] A. F. Young, J. D. Sanchez-Yamagishi, B. Hunt, S. H. Choi, K. Watanabe, T. Taniguchi, R. C. Ashoori, and P. Jarillo-Herrero, Nature (London) **505**, 528 (2014).
[10] P. Stepanov, S. Che, D. Shcherbakov, J. Yang, R. Chen, K. Thilahar, G. Voigt, M. W. Bockrath, D. Smirnov, K. Watanabe, T. Taniguchi, R. K. Lake, Y. Barlas, A. H. MacDonald, and C. N. Lau, Nat. Phys. **14**, 907 (2018).
[11] D. A. Abanin, P. A. Lee, and L. S. Levitov, Phys. Rev. Lett. **96**, 176803 (2006).
[12] A. Roth, C. Brune, H. Buhmann, L. W. Molenkamp, J. Maciejko, X.-L. Qi, and S.-C. Zhang, Science **325**, 294 (2009).
[13] J. C. Leutenantsmeyer, A. A. Kaverzin, M. Wojtaszek, and B. J. van Wees, 2D Mater. **4**, 014001 (2016).
[14] P. Wei, S. Lee, F. Lemaitre, L. Pinel, D. Cutaia, W. Cha, F. Katmis, Y. Zhu, D. Heiman, J. Hone, J. S. Moodera, and C.-T. Chen, Nat. Mater. **15**, 711 (2016).
[15] H. X. Yang, A. Hallal, D. Terrade, X. Waintal, S. Roche, and M. Chshiev, Phys. Rev. Lett. **110**, 046603 (2013).
[16] Z. Qiao, W. Ren, H. Chen, L. Bellaiche, Z. Zhang, A. H. MacDonald, and Q. Niu, Phys. Rev. Lett. **112**, 116404 (2014).
[17] A. Hallal, F. Ibrahim, H. Yang, S. Roche, and M. Chshiev, 2D Mater. **4**, 025074 (2017).
[18] J. Lee and J. Fabian, Phys. Rev. B **94**, 195401 (2016).
[19] Z. Wang, C. Tang, R. Sachs, Y. Barlas, and J. Shi, Phys. Rev. Lett. **114**, 016603 (2015).
[20] N. G. Kovalchuk, K. A. Nigerish, M. M. Mikhalik, N. I. Kargin, I. V. Komissarov, and S. L. Prischepa, J. Appl. Spectrosc. **84**, 995 (2018).
[21] See Supplemental Material at http://link.aps.org/supplemental/10.1103/PhysRevB.101.241405 for the detailed device fabrication and characterization, extrinsic origins of nonlocal resistance, and the theoretical description of the magnetic phase transition.
[22] V. T. Phong, N. R. Walet, and F. Guinea, 2D Mater. **5**, 014004 (2017).
[23] D. A. Abanin, S. V. Morozov, L. A. Ponomarenko, R. V. Gorbachev, A. S. Mayorov, M. I. Katsnelson, K. Watanabe, T. Taniguchi, K. S. Novoselov, L. S. Levitov, and A. K. Geim, Science **332**, 328 (2011).